

Structural phase transitions and stress accommodation in $(\text{La}_{0.67}\text{Ca}_{0.33}\text{MnO}_3)_{1-x}:(\text{MgO})_x$ composite films

O. I. Lebedev,* J. Verbeeck, and G. Van Tendeloo

EMAT, University of Antwerp (RUCA), Groenenborgerlaan 171, B-2020 Antwerp, Belgium

O. Shapoval and A. Belenchuk

Institute of Applied Physics, Academiei str. 5, MD-2028 Kishinev, Moldova

V. Moshnyaga, B. Damashcke, and K. Samwer

1. Physikalisches Institut, Universität Göttingen, Bunsenstrasse 9, D-37073 Göttingen, Germany

(Received 8 January 2002; revised manuscript received 23 April 2002; published 24 September 2002)

Composite $(\text{La}_{0.67}\text{Ca}_{0.33}\text{MnO}_3)_{1-x}:(\text{MgO})_x$ films were prepared by metalorganic aerosol deposition on a (100)MgO substrate for different concentrations of the (MgO) phase ($0 \leq x \leq 0.8$). At $x \approx 0.3$ a percolation threshold in conductivity is reached, at which an infinite insulating MgO cluster forms around the $\text{La}_{0.67}\text{Ca}_{0.33}\text{MnO}_3$ grains. This yields a drastic increase of the electrical resistance for films with $x > 0.3$. The film structure is characterized by x-ray diffraction and transmission electron microscopy. The local structure of the $\text{La}_{0.67}\text{Ca}_{0.33}\text{MnO}_3$ within the film depends on the MgO concentration which grows epitaxially along the domain boundaries. A different structural phase transition from the orthorhombic $Pnma$ structure to an unusual rhombohedral $R\bar{3}c$ structure at the percolation threshold $x \approx 0.3$ is found for $\text{La}_{0.67}\text{Ca}_{0.33}\text{MnO}_3$. A three-dimensional stress accommodation in thick films through a phase transition is suggested.

DOI: 10.1103/PhysRevB.66.104421

PACS number(s): 68.35.Rh, 75.60.Ch, 75.70.Cn

I. INTRODUCTION

The discovery of “colossal magnetoresistance” (CMR) in perovskite based rare-earth manganates of the type $\text{Ln}_{1-x}\text{A}_x\text{MnO}_3$ (Ln is rare earth, A is divalent cation)¹ has caused intense research activities over the last few years. In the following years, more remarkable properties (such as spin and charge ordering) have been discovered and studied by different techniques. It has been shown that the electronic and magnetic properties are strongly dependent on the chemical composition and the crystal structure.

Apart from the perovskite based materials, researchers are hunting for new types of material, showing a CMR effect. They have been found in the layered perovskites (Ruddlesden-Popper phases)² and in some pyrochlore type structures.³

The other direction is to induce various modifications to the basic $(\text{A}_{1-x}\text{A}'_x\text{BO}_3)$ structure by adopting different A rare-earth cations, by doping with A' cations and/or alter the oxygen stoichiometry. This will induce a different internal strain, due to rotation or/and distortion of the vertex-sharing MnO_6 octahedra. The strain in the structure is characterized by the Goldschmidt tolerance factor, defined as $\tau = [r_A + r_O] / \sqrt{r_B + r_O}$, where r are the ionic radii. A tolerance factor $\tau = 1$ corresponds to the unstrained cubic structure while $\tau \neq 1$ indicates a strained structure relaxed by a structural distortion from the ideal cubic structure. The structural phase diagram of $\text{A}_{1-x}\text{A}'_x\text{MnO}_3$ ($\text{A} = \text{La, Pr, Y, \dots}$; $\text{A}' = \text{Ca, Sr, Ba} \dots$) as a function of the average A -site ionic radius was reported by Radaelli *et al.*⁴ It was shown that the structure and the corresponding physical properties can be tuned by changing the average radius (r_A) of the A cation.

Thin films of manganite oxides grown epitaxially on a substrate give a unique opportunity to induce different types of perovskite distortions by creating different stress fields resulting from the lattice mismatch with the substrate. The magnitude and the sign of the stress (compressive or tensile) in a film depends on the substrate-film lattice misfit and thus can be adjusted by the choice of the substrate. This opens the possibility to design new types of the structures with predictable physical properties.

This was shown by Locquet *et al.*⁵ for copper-oxide superconductors and later for CMR properties in $\text{La}_{1-x}\text{Sr}_x\text{MnO}_3$ thin films.^{6,7} A field-induced insulator-to-metal transition below 240 K in $\text{Pr}_{0.5}\text{Ca}_{0.5}\text{MnO}_3$ thin films grown on (100)STO was reported by W. Prellier *et al.*⁸ and associated with an effect of the tensile stress. Biswas *et al.*⁹ show that thin $\text{La}_{0.67}\text{Ca}_{0.33}\text{MnO}_3$ films grown under a small compressive strain ($\approx 2\%$) are structurally, magnetically, and electronically nonuniform due to island growth. This leads to coexistence of two different phases, a metallic ferromagnet and an insulating antiferromagnet.

Recently, composite bulk samples of $\text{La}_{0.7}\text{Ca}_{0.3}\text{MnO}_3$ (LCMO) and $\text{La}_{0.7}\text{Sr}_{0.3}\text{MnO}_3$ (LSMO) were shown to be interesting systems in which the electron transport can be affected to a large extent by the presence of a second phase. For example, an enhancement of the low-field magnetoresistance (MR) at room temperature for an LSMO-glass composite at the percolation threshold of conductivity was demonstrated.⁷

Thin-film composites seem to be promising not only for the realization of a low-field MR material, but one can consider them also as model systems. Here an artificial chemical phase separation results in a corresponding electronic (metal-

TABLE I. Characteristics of $(\text{LCMO})_{1-x}:(\text{MgO})_x$ composite films.

x	0	0.01	0.05	0.1	0.33	0.5	0.67	0.8
T_{MI} (K)	257	260	205	149				
T_C (K)	260	245	197	145	228	216	210	208
CMR (%)		700	1400	15000	90000			
c (nm)	0.385(8)	0.386(3)	0.386(7)	0.387(4)	0.388(0)	0.389(3)	0.391(4)	0.394(8)

insulator) or/and magnetic (ferromagnetic-antiferromagnetic) phase separation. The parameters of such an “electronic phase separation” can be remarkably controlled by the processing conditions and its scale can be very fine, down to a few nanometers. The magnetotransport in such a model system can be compared with that recently observed in ferromagnetic metal/antiferromagnetic insulator phase separated systems.^{10,11}

Not only can the properties to a large extent be controlled but also the structure of the film can be designed by means of the surrounding second phase. This becomes particularly interesting when both phase constituents grow epitaxially on the substrate. Such epitaxial composite films will be considered as a starting point for the study of the structure-property relationships in three-dimensional (3D) clusters of manganites embedded in an appropriate oxide matrix.

The aim of the present paper is a structural investigation of the $(\text{La}_{0.67}\text{Ca}_{0.33}\text{MnO}_3)_{1-x}:(\text{MgO})_x$ [$(\text{LCMO})_{1-x}:(\text{MgO})_x$] composite thin films grown on an MgO(100) substrate (misfit is around 8%). The epitaxial $(\text{LCMO})_{1-x}:(\text{MgO})_x$ composite films were prepared over a large range of the second phase concentration $0 \leq x \leq 0.8$ and structural as well as magnetotransport changes of LCMO were observed as function of the MgO content. A different structural phase transition from the orthorhombic ($Pnma$) LCMO structure to an unusual (most probably rhombohedral $R\bar{3}c$) structure at the percolation threshold $x_c \approx 0.3$ is found. The structural changes are usually so small that powerful methods such as transmission electron microscopy (TEM) and particularly high-resolution electron microscopy (HREM) are required for a detailed characterization.

II. EXPERIMENTAL METHODS

A. Sample preparation

$(\text{LCMO})_{1-x}:(\text{MgO})_x$ films were prepared by a metalorganic aerosol deposition described elsewhere.¹² This is a solution based technique which uses a mixture of the corresponding metal-chelate precursors dissolved in an organic solution. The deposition of oxide films occurs as a result of heterogeneous pyrolysis of finely dispersed aerosol/vapor phase of metalorganic precursors on the heated substrate. To obtain composite films an appropriate amount of Mg precursor is added to the basic solution used for the preparation of LCMO films. Thus a simultaneous growth of LCMO and MgO phases from a single precursor solution is realized. The nominal concentration “ x ” of the insulating MgO phase in the composite films corresponds to the molar concentration of the Mg precursor in the precursor solution. Freshly

cleaved MgO(100) single-crystalline plates are used as substrates. The substrate temperature during the film deposition was 700 °C and the deposition rate was about 40 nm/min. The final thickness of the films was in the range 150–200 nm.

B. Characterization methods

The macrostructure of the films is characterized by x-ray diffraction (XRD) using $\text{CuK}\alpha$ radiation, on a Siemens D5000 diffractometer. As was established by XRD the films were epitaxially grown on MgO substrate with relations $\text{LCMO}(001)\parallel\text{MgO}(100)$, i.e., with the c axis perpendicular to the substrate plane.¹³ At that the pseudocubic c -axis lattice parameter of the LCMO depends significantly on the MgO concentration x (see also Table I).

The microstructure of the films is studied by TEM and high-resolution electron microscopy (HREM) for plan view and cross-section geometries of the samples. Electrical transport properties are measured by the four-probe dc method in a temperature range from 4.2 to 300 K and under magnetic fields ranging from 0 to 5 T. A commercial He cryostat equipped with a superconducting solenoid (Cryogenics Ltd.) is used. Magnetization measurements are carried out by means of a vibrating sample magnetometer (VSM) as well as by a commercial superconducting quantum interference device magnetometer at $T = 1.8\text{--}300$ K with the magnetic field aligned parallel to the substrate. Transport measurements on identical specimens were reported earlier.¹³

TEM investigations are carried out with a JEOL 4000EX microscope operated at 400 kV. The point resolution of the microscope is of the order of 0.17 nm. Cross-section as well as plan view specimens for TEM study are prepared by the standard techniques: mechanical polishing to a thickness of about 15 μm followed by ion milling under grazing incidence. The phase composition of the LCMO film, and in particular the cation ratio, were determined by EDX analysis of the LCMO grains in a Philips CM20 microscope with a LINK-2000 attachment. For the EDX analysis plan view specimens were used and results are based on the La(L), Ca(K) and Mn(K) lines in the spectra. The cation ratio, as determined by EDX, is found close to the expected composition of La:Ca:Mn=0.7:0.3:1.0.

The energy filtered TEM (EFTEM) technique is used to create elemental maps of Mg with the standard three-window technique.¹⁴ EFTEM images are captured using a Gatan GIF2000 coupled to a Philips CM30 FEG. Maps of the Mg K -edge, La $M_{4,5}$ -edge, Mn $L_{2,3}$ -edge, Ca K -edge and O K -edge are acquired to confirm the chemical composition of the sample. Both cross-section and plan view specimens are checked with qualitatively EFTEM. The collection angle is 19.2 mrad and the exposure time for the Mg K -edge is 60 s.

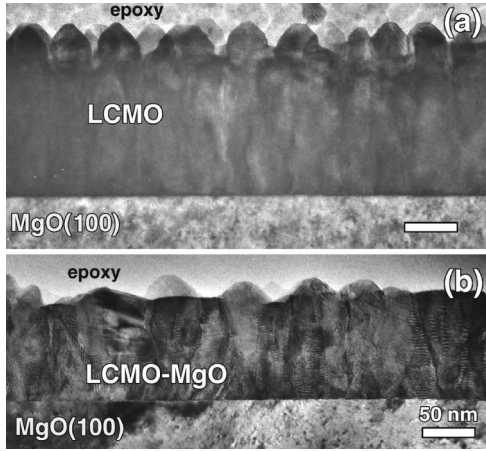


FIG. 1. Low magnification multibeam images of cross-section samples of as-grown $(\text{La}_{0.67}\text{Ca}_{0.33}\text{MnO}_3)_{1-x}:(\text{MgO})_x/\text{MgO}(100)$ with different MgO concentration: (a) $x=0$; (b) $x=0.33$.

The sample orientation is chosen to be slightly off axis to reduce problems with diffraction contrast. Drift between the three window images is corrected by cross correlation.

C. Structural considerations

As already mentioned above, the structure of a film can be different from that of the bulk due to stress resulting from the lattice mismatch. The deviations from the bulk structure, however, are likely to be small.

Bulk $\text{La}_{1-x}\text{Ca}_x\text{MnO}_3$ has a deformed perovskite structure for all x values and is described by the orthorhombic space-group $Pnma$ with lattice parameters $a_o \approx c_o \approx a_p\sqrt{2}$ and $b_o \approx 2a_p$,^{4,15-17} where a_p is the perovskite mesh. Recently, Lobanov *et al.*¹⁸ reported neutron powder-diffraction data for $\text{La}_{0.85}\text{Ca}_{0.15}\text{MnO}_3$ where a monoclinic distortion of the GdFeO_3 -type structure [SG $P2_1/c$; $a_m = 0.774476(6)$ nm; $b_m = 0.550398(4)$ nm and $c_m = 0.547351(4)$ nm, $\beta = 90.091^\circ$] was revealed. The crystal structure exhibits a specific ordering of the Mn-O apical distances with nonequivalent MnO_2 layers alternating along the a axis. The deviation from the $Pnma$ structure, however, is extremely small. In our calculations we will use the $Pnma$ unit cell with lattice parameters $a_o = 0.5481(8)$ nm, $b_o = 0.7751(5)$ nm, and $c_o = 0.5499(6)$ nm.

The MgO substrate has a cubic structure $Fm\bar{3}m$ $a = 4.220$.¹⁹ The misfit d along the interface is defined as $\delta = (a_{\text{MgO}} - a_{\text{LCMO}})/a_{\text{MgO}}$, which in the present case is $\delta \approx 8\%$.

III. EXPERIMENTAL RESULTS

A. Low-magnification TEM

Cross-section multibeam bright field images of $(\text{LCMO})_{1-x}:(\text{MgO})_x$ composite films for $x=0$ and $x=0.5$ are shown in Fig. 1. Films are epitaxial at all MgO concentrations and exhibit sharp well defined film/substrate interfaces. The thickness of the film is 120–150 nm. All films show the presence of a columnar microstructure with col-

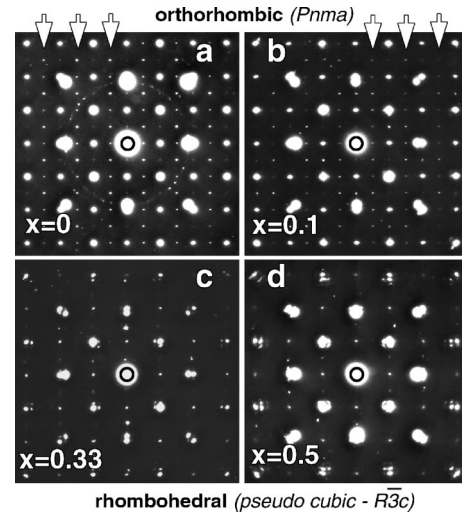


FIG. 2. Electron-diffraction patterns cross-section samples for different MgO concentrations: (a) $x=0$; (b) $x=0.1$; (c) $x=0.33$; (d) $x=0.5$. The white arrows in (a) and (b) indicate reflections specific for the $Pnma$ space group. These spots are absent in (c) and (d).

umns parallel to the interface normal, but the grain boundary and surface structure of the films vary with the MgO composition.

A pure LCMO film ($x=0$) exhibits an almost uniform domain size around 40 nm [Fig. 1(a)]. The uniform contrast of the domains and domains boundaries suggests that no secondary phase is present at the boundaries. The surface of the film is not flat and pyramidlike grains separating different domains are clearly visible. The possible origin of this shape will be further discussed.

The microstructure of composite films ($x>0$) changes with x . The film surface grows flatter with increasing MgO content; moreover the domains size changes. At the column boundaries Moiré patterns appear [Fig. 1(b)]. They start from the interface film/substrate and run through the film to the surface. These Moiré patterns are related to the presence of MgO as a second phase. The LCMO-MgO overlap along the viewing direction and because of the lattice mismatch Moiré patterns are formed. The width of the Moiré regions increases with increasing MgO content.

Diffraction patterns from cross-section specimens are the superposition of diffraction patterns produced by film and substrate; they clearly show a variation with increasing MgO content (Fig. 2). All patterns can be indexed as a composite of two materials: LCMO and MgO. The electron-diffraction (ED) pattern obtained from the pure LCMO film ($x=0$) [Fig. 2(a)] can be indexed with respect to an orthorhombic lattice ($Pnma$, $a_o = a_p\sqrt{2}$, $b_o = 2a_p$, $c_o = a_p\sqrt{2}$). Two different domain orientations ($[010]^*$ and $[101]^*$) are present within the selected area and oriented with the following epitaxial relationship:

$$(100)_{\text{MgO}} \parallel (010)_{\text{LCMO-O}} \cdot [100]_{\text{MgO}} \parallel [\bar{1}01]_{\text{LCMO-O}}$$

$$\text{or } (100)_{\text{MgO}} \parallel (\bar{1}01)_{\text{LCMO-O}} \cdot [100]_{\text{MgO}} \parallel [010]_{\text{LCMO-O}}$$

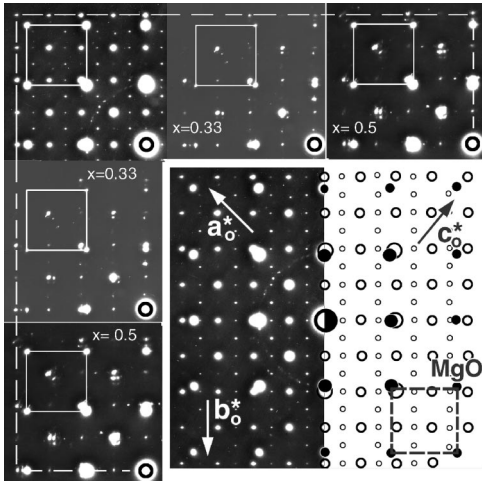


FIG. 3. Magnified left upper quadrants of the cross-section ED patterns (see Fig. 2): initial $x=0$, $x=0.33$, and $x=0.5$. The white squares indicate the position of the MgO substrate spots. The spot splitting due to the superposition of the MgO and LCMO pattern is clearly visible. The magnitude of the splitting is equal along both orthogonal directions.

Increasing the MgO concentration to $x=0.1$ does not lead to visible changes of the ED patterns [Fig. 2(b)]. The reciprocal rows, indicated by white arrows in Figs. 2(a) and (b), however, disappear for $x=0.33$ [Figs. 2(c) and (d)]. This suggests a different space group. The diffraction conditions of $R\bar{3}c$ are consistent with all observations for high MgO concentrations [Figs. 2(c) and (d)].

Enlargements of one-quarter of the diffraction patterns from three specimens and a schematic drawing of the cross-section ED pattern ($x=0$) are presented in Fig. 3. Black circles indicate the positions of the MgO reference reflections, while open circles correspond to the spots from the film. It is assumed that the lattice of the substrate does not depend on the MgO concentration in the LCMO composite film and that one can use the MgO reflections for internal calibration. The spot splitting due to the difference in lattice parameters between film and substrate is present along all directions of the ED pattern. Moreover, the magnitude of the spot splitting is constant and does not depend on the MgO concentration. This means that the cell parameters of LCMO do not depend on the MgO concentration. The slight streaking of the spots in the diagonal directions is a signature of the small misorientation of LCMO domains with respect to each other and to the MgO substrate.

Figure 4 is a multibeam diffraction contrast low magnification image of a plan view sample for $x=0.5$. The corresponding ED pattern (inset of Fig. 4) clearly shows that two different phases with a different lattice parameter are present in the film. The pattern can be interpreted based on the presence of both LCMO and MgO, viewed along a cube direction and oriented with the following relationship:

$$[001]_{\text{MgO}} \parallel [221]_{\text{LCMO-R}}; (010)_{\text{MgO}} \parallel (012)_{\text{LCMO-R}}.$$

The most intense spots represent the MgO reflections and weaker ones represent LCMO reflections. The complete pat-

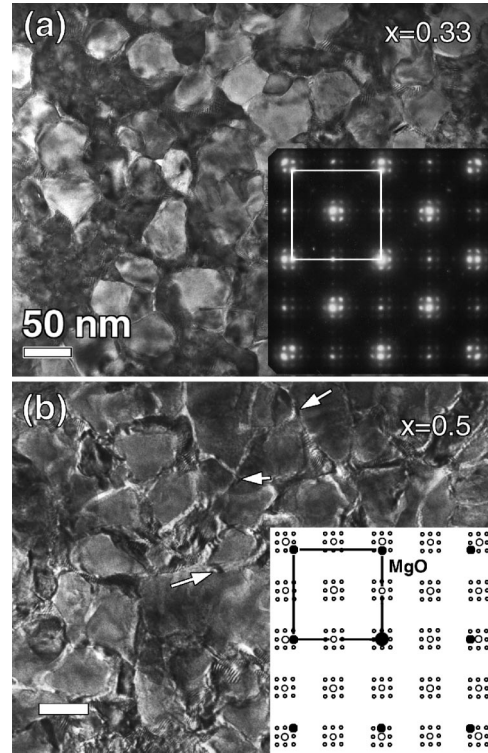


FIG. 4. Low magnification images of plan view samples for different MgO concentration: $x=0.33$ and $x=0.5$. The corresponding ED pattern and a schematic drawing are given as inset. The large black spots in this drawing represent MgO reflections; larger open circles represent LCMO reflections. Small open circles are due to double diffraction. The complete pattern results from double diffraction; the LCMO film acting as a secondary source.

tern results from the fact that all LCMO reflections act as secondary sources producing squares of double diffraction spots.

The microstructure of the film (Fig. 4) suggests that the film is formed by the coalescence of epitaxial columnar islands leaving a distinct intergranular contrast where the coalescing islands meet. The difference in brightness between different domains is due to a slight misorientation between them. The size of the grains and the structure of the domain boundaries depends on the MgO concentration. For MgO concentrations around 30% the grain size is about 40–50 nm. Only a few domain boundaries exhibit a bright contrast thin layer due to the presence of a secondary (MgO) phase at the boundary. Increasing the MgO concentration ($x=0.5$) leads to an increase of the grain size (about 50–80 nm), and the bright contrast layer around the LCMO grains becomes more dominant (indicated by arrows in Fig. 4). Since the presence of this material apparently does not affect the overall diffraction pattern (inset, Fig. 4), it is either amorphous or more probably isostructural with LCMO or MgO. The answer will be given by HREM.

B. High-resolution transmission electron microscopy

A HREM image taken across the interface shows that the LCMO film ($x=0$) grows epitaxial and is perfectly coherent

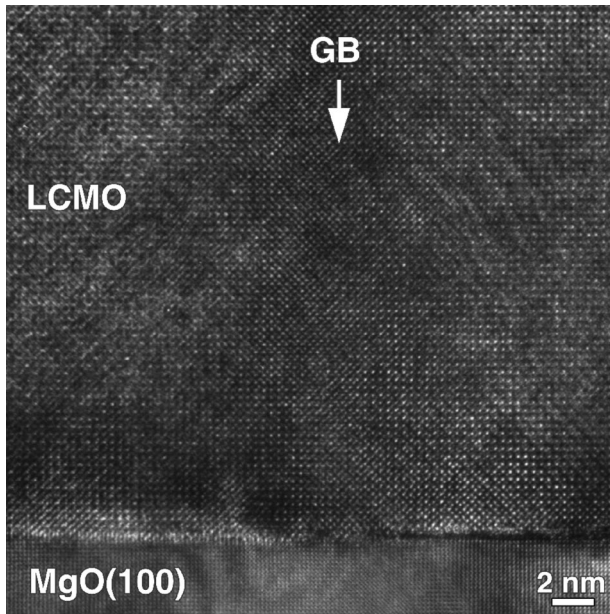


FIG. 5. Cross-section HREM image of the LCMO/MgO interface. The domain boundary is indicated by a white arrow. Note the absence of any intermediate layer or a secondary phase at the boundary.

across the interface. The LCMO/MgO interface is atomically sharp and flat. Along the LSMO/MgO interface interfacial edge-type dislocations, necessary to absorb the misfit, are formed. No secondary phase inclusions are observed either in the bulk of the film or along the interface. The domain boundaries in the LCMO film (easily observed in the low magnification of Fig. 1) are hardly visible in HREM images; only a slight difference in contrast is noticed (Fig. 5).

As the MgO concentration increases, the structure of the film changes. At low concentration of the MgO ($x=0.1$) no significant differences with the pure LCMO film are noticed and the structure remains perfectly coherent and free from secondary phases. Increasing the MgO concentration ($x=0.33-0.5$) leads to buckling of the film/substrate interface

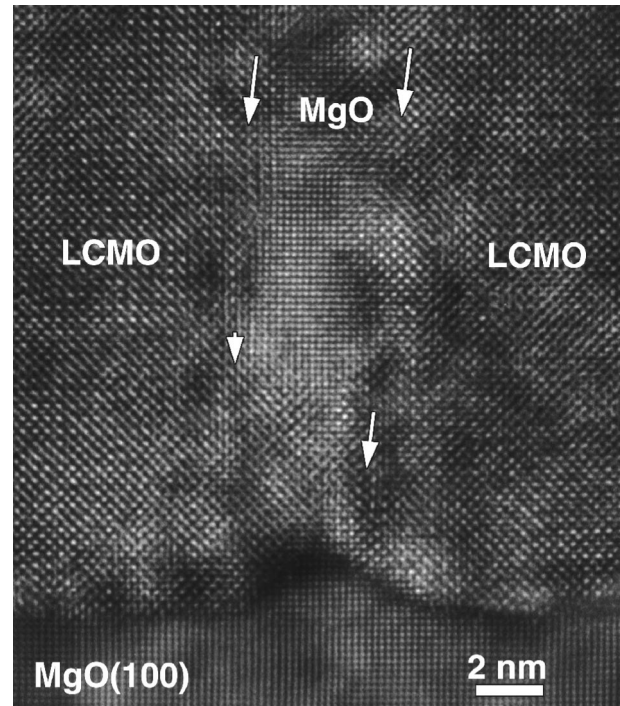


FIG. 6. Cross-section HREM image of the interface $(\text{La}_{0.67}\text{Ca}_{0.33}\text{MnO}_3)_{1-x}-(\text{MgO})_x/\text{MgO}(100)$ for $x=0.5$. Note the heteroepitaxial growth of MgO columns along a domain boundary in the direction parallel to the normal to the interface.

(Fig. 6) resulting from the epitaxial growth of MgO islands on the MgO substrate surface. The MgO layers start from the interface, grow along the original domain boundaries, and extend all the way through the film up to the surface. It is evident from the HREM image (Fig. 6) that the MgO layer is epitaxially intergrown between the LCMO domains with the same orientation as the MgO substrate. No amorphous phase is observed in the domain boundaries.

Plan view HREM observations confirm the epitaxial intergrowth of MgO along the domain boundaries. It is clear from the HREM plan view images (Fig. 7) that the bright contrast lines along the domain boundaries in Fig. 4 corre-

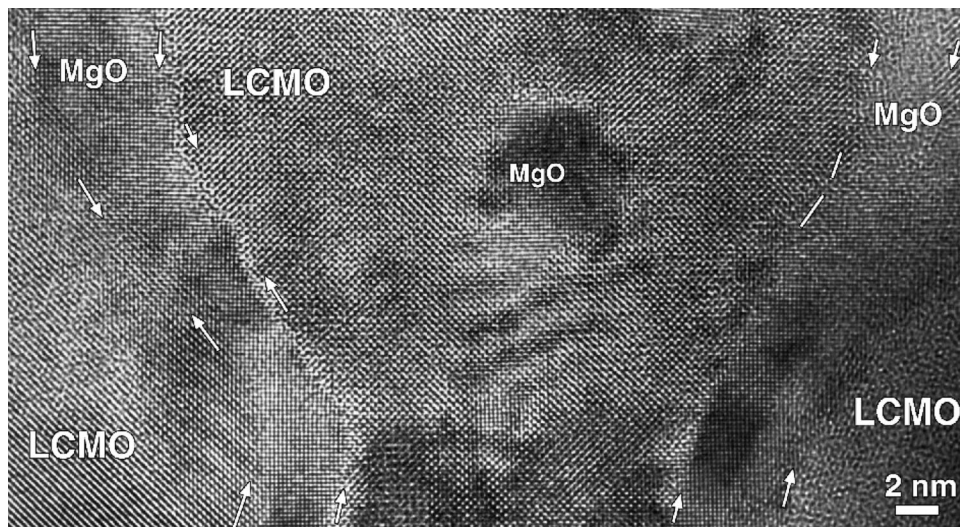


FIG. 7. Plan view HREM image of the interface $(\text{La}_{0.67}\text{Ca}_{0.33}\text{MnO}_3)_{1-x}-(\text{MgO})_x/\text{MgO}(100)$ for a sample with $x=0.5$. Note the epitaxial growth of the MgO layer around LCMO grains.

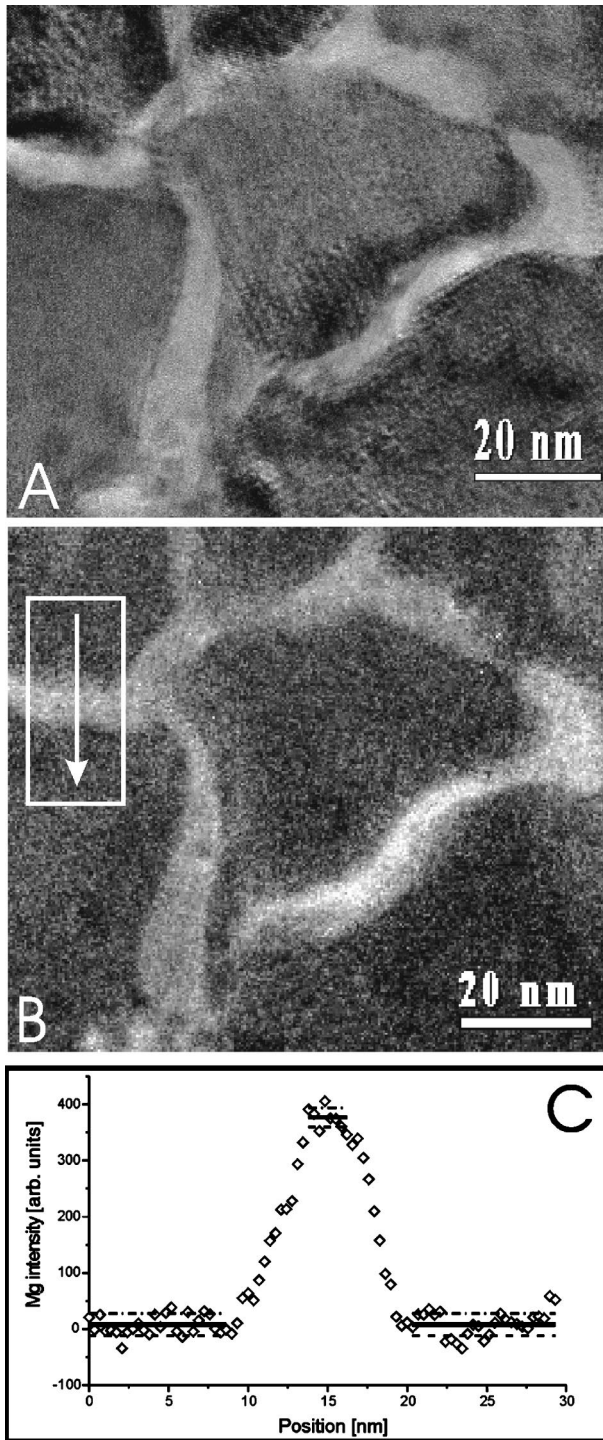


FIG. 8. Zero-loss filtered TEM image (a) and the elemental Mg map (b). The integrated line scan across the MgO layer in the white rectangle and in the direction indicated by the arrow is shown in (c).

spond to the epitaxial MgO layers around the LCMO grains. The interface between the LCMO grain and the MgO layer is not straight and has no specific crystallographic orientation. This explains the presence of the Moiré patterns on the TEM images of Fig. 1(b), which are due to the overlap of two different structures: LCMO and MgO.

C. Energy filtered transmission electron microscopy

Figure 8(b) shows the Mg elemental map from a plan view specimen with the accompanying zero-loss filtered image [Fig. 8(a)]. The elemental map shows a good localization of the Mg signal in the bright columnlike features of the zero-loss image. An integrated line scan across a MgO tube wall [Fig. 8(c)] shows that the Mg signal drops rapidly to zero on both sides of a MgO wall. As a rough estimate for the upper limit of Mg in the LCMO grain, we calculate the standard deviation in the region outside and inside the wall from the profile in Fig. 8. We take into account the bright field intensity difference between the two regions and get an estimate for an upper bound of around 7% for the Mg concentration per volume in the LCMO layer as compared to the MgO wall. This accuracy is on the order of what is to be expected from the three-window elemental mapping technique.

From the EFTEM results, we conclude that there is no observable diffusion of Mg into the LCMO domains within the expected error of the three-window technique. This result is in accordance with the fact that no structural data have been published on Mg substituted La-Ca-Mn-O phases. Some groups show that a moderate Mg doping (5–6%) of the La-Sr-Mg-Mn-O and La-Mn-Mg-O structure can be responsible for its properties and structural phase transition.^{20,21} These structures are also based on the perovskite structure and are similar to La-Ca-Mn-O. However, the authors do not report any structural data. In our experiments, we did not observe any structural phase transition (see Fig. 2) for 10% doping when it should be drastic according to the A. Anane *et al.*²⁰ and J. H. Zhao *et al.*²¹ It indicates that the Mg substitution mechanism is probably different in the La-Ca-Mn-O system compared to the La-Sr-Mn-O or La-Mn-O system and the idea of Mg (small ion size, 0.66 Å) substitution on a La or/and Ca (bigger ion size, 0.99 Å) sublattice is highly unlikely.

IV. MAGNETOTRANSPORT PROPERTIES

We have observed that electrical as well as magnetic characteristics change systematically as a function of the MgO content in composite $(\text{LCMO})_{1-x}(\text{MgO})_x$ films. In Table I the data on the metal-insulator transition temperature T_{MI} , the Curie temperature T_C , as well as maximal $CMR = 100\% R(0) - R(5 \text{ T})/R(5 \text{ T})$ and pseudocubic c -lattice parameters measured by x-ray diffraction are presented for films with $0 \leq x \leq 0.8$.

A pure LCMO ($x=0$) film is characterized by $T_M \approx T_C = 260 \text{ K}$ typical for the La-Ca-Mn-O manganite with a Ca doping of 0.33. These data along with the low residual resistivity $\rho(4.2 \text{ K}) \approx 10^{-4} \Omega \text{ cm}$ of the pure LCMO film allow us to conclude that the films prepared by the metalorganic aerosol deposition technique behave as an intrinsic LCMO material similar to the epitaxial films prepared by pulsed laser deposition (PLD) method. Moreover, the value of the c -lattice parameter, $c = 0.385(8) \text{ nm}$, is close to the corresponding bulk value and indicates no mechanical stress in pure LCMO films.

Upon increasing the MgO concentration in the region

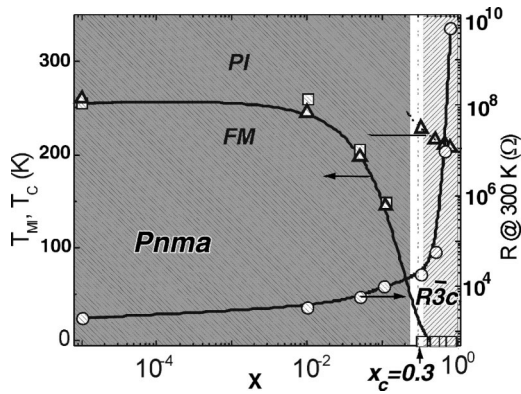


FIG. 9. The dependences of the Curie temperature (triangle) T_C , (K) and the metal-insulator transition temperature (square) T_{MI} , (K), and room-temperature resistance (circle) R , [(Ω) right scale] on the concentration “ x ” of the MgO phase in composite films.

$0 < x < 0.3$ the values of T_{MI} and T_C for composite films decrease systematically, while $CMR = 100\% [R(0) - R(5 \text{ T})]/R(5 \text{ T})$ becomes extremely pronounced, reaching about $10^5\%$. Such a magnetotransport behavior is in a good accordance with that found previously for coherently strained LCMO films deposited on SrTiO_3 or LaAlO_3 substrates.^{1,22,23} The c -lattice parameter increases significantly up to 0.388(8) nm for $x = 0.33$, indicating the development of stress in composite films with increasing MgO content.

At $x \approx 0.3$ the percolation threshold in conductivity takes place, at which an infinite insulating MgO cluster forms yielding a drastic increase of the electrical resistance for films with $x > 0.3$. The value of the percolation threshold is in good agreement with that observed in LSMO-glass bulk composites.⁷ Remarkably, that the $Pnma-R\bar{3}c$ structural phase transition takes place also for $x \approx 0.3$; i.e., the structural phase transition is coupled to the percolation threshold. The reason seems to be a drastic increase of the 3D stress contribution when all the LCMO domains are surrounded by epitaxially grown MgO layers. This happens exactly at the percolation threshold. The magnetotransport data for composite films are summarized in a phase diagram shown in Fig. 9, which illustrates the relationship between the microscopic structure and the macroscopic properties (resistance and magnetization). Note that T_C has a nonmonotonous dependence on “ x ” with a minimum at x_C and a further increase in the $R\bar{3}c$ phase.

V. GROWTH MECHANISM

A possible growth mechanism for composite $(\text{LCMO})_{1-x}:(\text{MgO})_x$ films can be suggested based on the present experimental observations. It is schematically shown in Fig. 10.

As mentioned before, the pseudocubic lattice parameter of LCMO is much smaller than that of MgO (misfit $\approx 8\%$) suggesting a three-dimensional (3D) island growth mode. At the formation temperature (700 °C) small islands of LCMO and

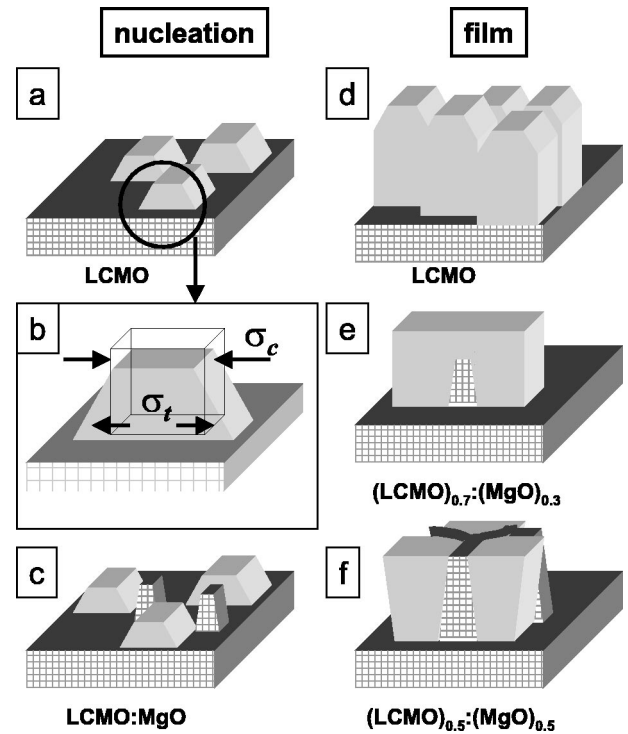


FIG. 10. Schematic representation of the growth mechanism of the composite film at different stages: (a) Nucleation of the LCMO film on the MgO substrate. (b) Enlargement of one LCMO island on the MgO substrate. The ideal shape of the island when no stress is present is shown by the cube frame. Close to the interface the LCMO region is under a two-dimensional tensile stress (σ_t); the upper part of the LCMO island is under a two-dimensional compressive stress (σ_c). The shape of LCMO becomes pyramidal. (c) Nucleation of the $(\text{LCMO})_{1-x}:(\text{MgO})_x$ composite film on the MgO substrate. Note the separate growth of LCMO and MgO islands. (d) The columnar structure of the LCMO film on the MgO substrate. Note the pyramidal shape of the surface of each separate LCMO domain. (e) Structure of the $(\text{LCMO})_{1-x}:(\text{MgO})_x$ film for $x = 0.33$. Intergrowth of the MgO islands in between LCMO domains occurs. Because of the low MgO content, the MgO layer does not reach the film surface. (f) Structure of the $(\text{LCMO})_{1-x}:(\text{MgO})_x$ film for $x = 0.5$. Every LCMO grain is surrounded by MgO through the complete film thickness.

MgO appear epitaxially on the MgO substrate surface [Figs. 10(a) and (c)]. Since the MgO grains have the same structure as the substrate no misfit strain is present at the interface. The situation with LCMO, however, is different and the LCMO islands grains are under a tensile strain ($a_{\text{LCMO}} < a_{\text{MgO}}$) [Fig. 10(b)]. Since the epilayer is much thinner than the substrate we assume that the strain is completely taken up in the epilayer. The epilayer is thus in a state of tensile biaxial “surface stress” in the $[100]_{\text{MgO}}$ and $[010]_{\text{MgO}}$ directions along the interface, which in isotropic elasticity is given by

$$\sigma = \frac{2\mu(1+\nu)}{1-\nu}, \quad (1)$$

where μ and ν are the shear modulus and Poisson ratio in the epilayer. The elastic strain energy of the epilayer per unit area is²⁴

$$E_s = \frac{2\mu(1+\nu)}{(1-\nu)\sigma^2 h}, \quad (2)$$

where h is the film thickness.

Upon growth of the island, transformation stresses, due to the tendency of the structure to adopt the bulk structure of LCMO, are now superimposed on the misfit stress. The upper surface of the islands therefore feel a compressive stress [Fig. 10(b)]. Such variation of strain within a single island is responsible for the pyramidal shape of the LCMO domain surface when no secondary phase (MgO) is present. In the next growth stage, the LCMO grains are connected by domain edges creating a configuration as in Fig. 10(d). The misfit between the MgO substrate and the LCMO film is responsible for the surface grain morphology and also influences the size of the domains.

In the case of composite film growth ($x > 0$), two island types nucleate in the initial stage: MgO and LCMO. As we already mentioned, the MgO islands grow free of stress while the LCMO islands are under a tensile stress [Fig. 10(b)]. They are randomly distributed on the substrate surface [Fig. 10(c)] and the ratio between the different types only depends on the MgO concentration in the film. When the LCMO and MgO nuclei grow, they will touch and the MgO islands will create a wall around the LCMO domains [Figs. 10(e) and (f)]. The MgO material with a cubic structure acts as a matrix for epitaxial LCMO growth inside the ‘‘MgO box.’’ As a result the 3D uniform stress becomes predominant making the strain variation in LCMO domains negligible. This leads to a different mechanism of misfit accommodation.

VI. DISCUSSION

The elastic stress analysis of an epilayer grown on a flat substrate with slightly different lattice parameters was done by Frank and van der Merwe²⁵ and by Jesser and Kuhlmann-Wilsdorf.²⁶ It was demonstrated that once the thickness of the epilayer exceeds a certain critical thickness it becomes energetically favorable to introduce stress annihilating dislocations at the interface to relieve the elastic strain energy [see Eq. (2)]. However, in perovskite-type structures several other mechanisms of stress relieve in an epitaxial film have been found in recent years: a breakdown of symmetry from orthorhombic to monoclinic,²⁷ the formation of prismatic antiphase domains or the formation of pseudoperiodical microtwins.²⁸ In the following we will suggest a different type of 3D stress accommodation in thick films through a phase transition from a low to a higher group symmetry.

It is well known that phase transitions in crystals are usually accompanied by changes in symmetry. According to the Landau theory, the space group of the low-temperature phase should be a subgroup of the space group of high-temperature phase. Since pressure has a similar effect as temperature, we can apply these rules for our particular case. Our experimental observations, particularly electron-energy-loss spectroscopy (EELS) and HREM data, suggest that only the internal pressure resulting from the epitaxial intergrowth of the MgO

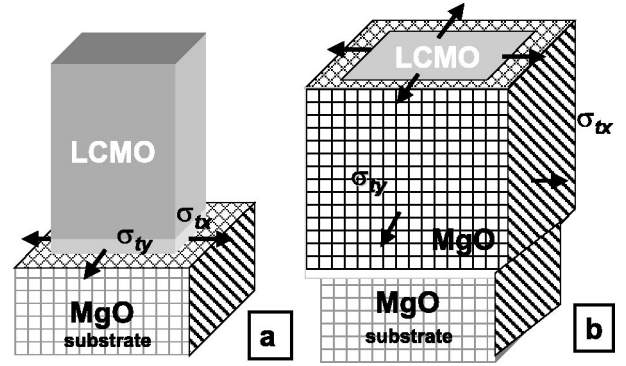


FIG. 11. Schematic representation of (a) a single LCMO domain on MgO, (b) a $(\text{LCMO})_{1-x}:(\text{MgO})_x$ composite film. The LCMO-MgO grain is under a 3D stress due to the MgO surrounding matrix; a 2D surface stress is present in the area close to the LCMO/MgO interface.

columns within the LCMO film cause the $Pnma$ -to- $R\bar{3}c$ phase transition in $\text{La}_{0.67}\text{Ca}_{0.33}\text{MnO}_3$. This means that in our particular case we induce a phase transition from a low-pressure (low-temperature) $Pnma$ (62) phase to a high-pressure (high-temperature) $R\bar{3}c$ (167) phase.

For the phase transition to take place, the free energy of the new state should be lower than the free energy of the initial state. Strain energy plays a vital role in the nucleation of solid-state phase changes and the free energy of a system can be simply described as

$$E = E_s + E_v, \quad (3)$$

where E is the free energy of the system, E_s the surface energy which is determined by the misfit stress at the interface, and E_v the volume energy of the bulk. When a pure LCMO film grows on a Mg substrate, the usual stress accommodation for thick film takes place. The islands have free surfaces and the surface energy should be minimum [Fig. 11(a)]. The surface energy of the epilayer is given by Eq. (2) and increases linearly with thickness (h). At a critical thickness, it becomes energetically favorable to introduce interfacial dislocations, which absorb the stress. In the elastically strained state the interface is fully coherent. The presence of interfacial edge-type dislocations was indeed observed along the interface (Fig. 5). The volume free energy in this case will be minimal because no external pressure occurs in the system and the film structure adapts the more energetically stable form of the bulk material. This is exactly the case for $\text{La}_{0.67}\text{Ca}_{0.33}\text{MnO}_3$ which has a $Pnma$ space group according to the phase diagram.⁴ There is no contribution of the stress energy from the grain boundaries because the LCMO grains show a perfectly epitaxial intergrowth.

The $(\text{LCMO})_{1-x}:(\text{MgO})_x$ composite growth can be considered as the growth of a different phase (LCMO) within a matrix of a parent phase (MgO) [Fig. 11(b)]. The interface between the two phases creates a local increase of surface energy (E_s) when the first few atoms assemble in the new structure. The model of Fig. 11(b) assumes that the LCMO grains, differing from the MgO matrix in structure and in

composition, grow epitaxially on the MgO substrate and are surrounded by MgO matrix. The change of free energy, when a new phase of volume V and interface area A forms, causes an increase in elastic strain energy per unit volume of the new phase ΔE_v given as

$$\Delta E = V\Delta E_v + AE_s. \quad (4)$$

It is clear that the surface energy will drastically increase because of the increasing interface area (A_s). Moreover, the growth of the MgO layers [Fig. 10(f)] pushes two neighboring LCMO grains apart and creates an external stress within the bulk of the LCMO grains. The amount of stress directly depends on the thickness of the MgO layer which is determined by the MgO composition in the film. This external stress leads to an increase of the volume free energy of the LCMO material.

The surface energy can be partially reduced by introduction of dislocations into the interface raising the interfacial free energy and also by the introduction of small-angle grain boundaries. There is evidence of the latter in the ED patterns of Fig. 2 where a streaking of the spots in the radial direction is observed. The volume free energy can be decreased by a transition from a less stable to a more stable phase.

A final question is: towards which structure will the $Pnma$ LCMO transform? In other words, is it reasonable to suggest the unusual $R\bar{3}c$ structure, which does not exist for the bulk $\text{La}_{1-x}\text{Ca}_x\text{MnO}_3$ material?

The ideal perovskite structure AMO_3 belongs to the cubic space group $Pm\bar{3}m$. However, most perovskite based materials exhibit deviations from the ideal cubic symmetry. The most common deviations are induced by a tilting of the MO_6 octahedra.

Based on Glazer's²⁹ and recently Woodward's³⁰ analysis of tilt distortions in perovskites, the $Pnma$ structure of LCMO is described as $a^+a^-a^-$. The rotational displacement in the $R\bar{3}c$ structure on the other hand is described as $a^-a^-a^-$. Comparing these two structures, it is clear that the rhombohedral ($R\bar{3}c$) and the orthorhombic ($Pnma$) structures have the same topology as the primitive perovskite structure. They are different only by the sense and the magnitude of the tilt angles of the MnO_6 octahedra and possibly by the degree of deformation.²⁹ Both features may be influenced by an external stress field which is the case for the LCMO:MgO structure [Fig. 11(b)]. The LCMO domain is under the strong homogeneous 3D stress because of the surrounding epitaxial MgO matrix [Fig. 11(b)] while in the pure LCMO film [Fig. 11(a)] only a small 2D misfit stress is present. Actually, the rhombohedral ($R\bar{3}c$) structure can be considered as a pseudocubic structure which will perfectly fit the cubic MgO surrounding matrix. There is another candidate which would do the same: a cubic form with description $a^0a^0a^0$ where the octahedra do not tilt at all. However, there are several arguments against this choice. The first one is that the octahedra have to be tilted in the LCMO structure because of the substitution of La by a divalent cation.^{4,15,16} Also the lattice energy calculations made by Woodward³⁰ show that the $a^+a^-a^-$ and $a^-a^-a^-$ tilt systems have more

favorable lattice energies than the $a^0a^0a^0$. It therefore seems reasonable to accept that for a composite $(\text{LCMO})_{1-x}:(\text{MgO})_x$ film the $\text{La}_{0.67}\text{Ca}_{0.33}\text{MnO}_3$ structure undergoes a structural phase transition from $Pnma$ to $R\bar{3}c$ driven by the internal pressure.

A similar situation has been found in bulk $\text{La}_{0.7}(\text{Ca}_{1-y}\text{Sr}_y)_{0.3}\text{MnO}_3$ samples.^{17,31} Substituting Ca for Sr, which has a significantly larger ionic radius, leads to an increase of the internal chemical pressure, which is also negative in sign. At $x \approx 0.5$ a structural phase transition from the $Pnma$ structure to the $R\bar{3}c$ structure takes place. The latter structure is the normal structure for the pure $\text{La}_{0.7}\text{Sr}_{0.3}\text{MnO}_3$.

Remarkable is that the magnetotransport behavior in the vicinity of the structural phase transition in bulk $\text{La}_{0.7}(\text{Ca}_{1-y}\text{Sr}_y)_{0.3}\text{MnO}_3$ (Refs. 17 and 31) is very similar to that found in $(\text{LCMO})_{1-x}:(\text{MgO})_x$ composite films.¹³ Namely, an increase of the Curie temperature was observed in the $R\bar{3}c$ structure. However, the $T_C(x)$ dependence in composite films, depicted in Fig. 9, has a nonmonotonous character whereas the Curie temperature in bulk samples changes monotonically through the $Pnma$ - $R\bar{3}c$ phase boundary. The reason may be that the films in the $Pnma$ phase ($0 \leq x \leq 0.3$) suffer a mechanical stress, which tends to decrease T_C . In the $R\bar{3}c$ phase the stress is relieved and the Curie temperature increases up to the values comparable with the individual LCMO film, which shows no mechanical stress. This is also consistent with a known increase of the T_C values for the less distorted LSMO phase. The stress factor is absent for bulk samples of $\text{La}_{0.7}(\text{Ca}_{1-y}\text{Sr}_y)_{0.3}\text{MnO}_3$, which show a monotonous increase of T_C through the $Pnma$ - $R\bar{3}c$ structural phase transition.^{17,31}

Moreover, the colossal magnetoresistance in composite films was found to be largest, $\text{CMR} = \Delta R/R(5 \text{ T}) \approx 10^5\%$, for the film with $x = 0.33$. This is very close to the $Pnma$ - $R\bar{3}c$ phase boundary, which was found to coincide with the percolation threshold in conductivity. CMR in composite films is therefore realized as a field induced insulator-to-metal transition at which the infinite size of the metallic cluster can be achieved in a magnetic field of $B = 5 \text{ T}$.

VII. CONCLUSIONS

$(\text{La}_{0.67}\text{Ca}_{0.33}\text{MnO}_3)_{1-x}:(\text{MgO})_x$ composite films on a (100) MgO substrate have a microstructure and magnetotransport properties depending on the MgO concentration. The films exhibit a remarkable structure consisting of domains of LCMO material surrounded by an epitaxially intergrown MgO thin layer. This MgO layer creates a wall around the LCMO domains and as a result a uniform 3D stress is built up. A different type of 3D stress accommodation through a phase transition from a low to a high group symmetry has been proposed. Our experimental observations, and in particular EELS and HREM data, suggest that only the internal pressure resulting from the epitaxial intergrowth of the MgO columns within the LCMO film cause the $Pnma$ -to- $R\bar{3}c$ phase transition in $\text{La}_{0.67}\text{Ca}_{0.33}\text{MnO}_3$.

At $x \approx 0.3$ the percolation threshold in conductivity is

reached; it is not only accompanied by a drastic increase of the electrical resistance for films with $x > 0.3$ but also by the $Pnma-R\bar{3}c$ structural phase transition taking place in the LCMO. We therefore conclude that the structural phase transition is coupled to the percolation threshold. The reason seems to be a drastic increase of the 3D stress contribution when all the LCMO domains are surrounded by epitaxially grown MgO layers. This happens exactly at the percolation

threshold. The magnetotransport data for composite films are summarized in a phase diagram as shown in Fig. 9.

ACKNOWLEDGMENTS

This work was performed within the framework of IUAP V-1 of the Belgian government. The authors are indebted to Dr. A. Nikolaev for a helpful discussion.

*Electronic address: lebedev@ruca.ua.ac.be

- ¹S. Jin, T.H. Tiefel, M. McCormack, R.A. Fastnacht, R. Ramesh, and L.H. Chen, *Science* **264**, 413 (1994).
- ²Y. Moritomo, A. Asamitsu, H. Kuwahara, and Y. Tokura, *Nature (London)* **380**, 141 (1996).
- ³Y. Shimkawa, Y. Kubo, and T. Manako, *Nature (London)* **379**, 53 (1996).
- ⁴P. Radaelli, D. Cox, M. Marezio, S.-W. Cheong, P. Schiffer, and A. Ramirez, *Phys. Rev. Lett.* **75**, 4488 (1995).
- ⁵J.-P. Locquet, J. Perret, J. Fompeyrine, E. Mächler, J.W. Seo, and G. Van Tendeloo, *Nature (London)* **394**, 453 (1998).
- ⁶F. Razavi, G. Gross, H.-U. Habermeier, O.I. Lebedev, S. Amelinckx, G. Van Tendeloo, and A. Vigliante, *Appl. Phys. Lett.* **76**, 155 (2000).
- ⁷A. Gupta, X.W. Li, and G. Xiao, *Appl. Phys. Lett.* **78**, 1894 (2001).
- ⁸W. Prellier, A.M. Haghiri-Gosnet, B. Mercey, P. Lecoœur, M. Hervieu, C. Simon, and B. Raveau, *Appl. Phys. Lett.* **77**, 1023 (2000).
- ⁹A. Biswas, M. Rajeswari, R.C. Srivastava, Y.H. Li, T. Venkatesan, R.L. Greene, and A.J. Millis, *Phys. Rev. B* **61**, 9665 (2000).
- ¹⁰M. Uehara, S. Mori, C.H. Chen, and S.W. Cheong, *Nature (London)* **399**, 560 (1999).
- ¹¹A. Moreo, S. Yunoki, and E. Dagotto, *Science* **283**, 2034 (1999).
- ¹²V. Moshnyaga, I. Khoroshun, A. Sidorenko, P. Petrenko, A. Weidinger, M. Zeitler, B. Rauschenbach, R. Tidecks, and K. Samwer, *Appl. Phys. Lett.* **74**, 2842 (1999).
- ¹³V. Moshnyaga, B. Damaschke, K. Samwer, O. Shapoval, A. Belenchuk, O. Lebedev, J. Verbeeck, G. Van Tendeloo, M. Mueksch, V. Tsurkan *et al.* (unpublished).
- ¹⁴R. F. Egerton, *Electron Energy Loss Spectroscopy in the Electron Microscope*, 2nd ed. (Plenum Press, New York, 1996).
- ¹⁵P. Radaelli, D. Cox, L. Capogna, S.-W. Cheong, and M. Marezio, *Phys. Rev. B* **59**, 14 440 (1999).
- ¹⁶J. Blasco, J. Garcia, J.M. deTeresa, M.R. Ibarra, P.A. Algarabel, and C. Marquina, *J. Phys.: Condens. Matter* **8**, 7427 (1996).
- ¹⁷P. Radaelli, M. Marezio, H. Hwang, S.-W. Cheong, and B. Batlogg, *Phys. Rev. B* **54**, 8992 (1996).
- ¹⁸M. Lobanov, A. Balagurov, V. Pomjakushin, P. Fisher, M. Gutmann, A. Abakumov, O. D'yachenko, E. Antipov, O. Lebedev, and G. Van Tendeloo, *Phys. Rev. B* **61**, 8941 (2000).
- ¹⁹W. Bragg, *Nature (London)* **105**, 646 (1920).
- ²⁰A. Anane, C. Dupas, K. LeDang, J.P. Renard, P. Veillet, L. Pinsard, and A. Revcolevschi, *Appl. Phys. Lett.* **69**, 1160 (1996).
- ²¹J.H. Zhao, T. Song, H.P. Kunkel, X.Z. Zhou, R.M. Roshko, and G. Williams, *J. Phys.: Condens. Matter* **12**, 6903 (2000).
- ²²R. Vonhelmolt, J. Wecker, B. Holzapfel, L. Schultz, and K. Samwer, *Phys. Rev. Lett.* **71**, 2331 (1993).
- ²³K. Chahara, T. Ohno, M. Kasai, and Y. Kozono, *Appl. Phys. Lett.* **63**, 1990 (1993).
- ²⁴A. Sutton and R. Balluffi, *Interface in Crystalline Materials* (Clarendon Press, Oxford, 1995).
- ²⁵F. Frank and J. van der Merwe, *Proc. R. Soc. London, Ser. A* **198**, 205 (1949).
- ²⁶W. Jesser and D. Kuhlmann-Wilsdorf, *Phys. Status Solidi* **19**, 95 (1967).
- ²⁷O. Lebedev, G. Van Tendeloo, S. Amelinckx, B. Leibold, and H.-U. Habermeier, *Phys. Rev. B* **58**, 8065 (1998).
- ²⁸O.I. Lebedev, J. Verbeeck, G. Van Tendeloo, S. Amelinckx, F.S. Razavi, and H.U. Habermeier, *Philos. Mag. A* **81**, 2865 (2001).
- ²⁹A.M. Glazer, *Acta Crystallogr., Sect. B: Struct. Crystallogr. Cryst. Chem.* **B28**, 3384 (1972).
- ³⁰P.M. Woodward, *Acta Crystallogr., Sect. B: Struct. Sci.* **53**, 32 (1997).
- ³¹Y. Tomioka, A. Asamitsu, and Y. Tokura, *Phys. Rev. B* **63**, 024421 (2000).